Numerical Investigations of Small-Amplitude Disturbances in a Laminar Boundary Layer with Impinging Shock Waves

A. Pagella, U. Rist, S. Wagner
Institut für Aerodynamik und Gasdynamik, Universität Stuttgart
Pfaffenwaldring 21, 70550 Stuttgart, Germany

Summary

Two-dimensional shock/boundary-layer interactions on a laminar boundary layer over a flat plate at cold super- and hypersonic conditions have been computed in direct numerical simulations based on the complete Navier-Stokes equations. Comparison with both experimental and numerical data has shown good agreement for $Ma = 2$. For $Ma = 4.8$ and different shock strengths the steady flow-field is discussed and then stimulated with small perturbations. The perturbations are amplified already upstream of the shock in accordance to pressure and temperature gradients. Behind the point, where the shock hits the boundary layer, amplification reduces. Increasing shock angle causes separation and leads to higher amplification of the perturbations as well as larger non-parallel effects. To validate this observation, a laminar boundary layer without impinging shock is compared with linear stability theory and non-parallel effects are clearly identified.

1 Introduction

Transition to turbulence in high-speed boundary layers is not yet fully understood because of its higher complexity compared to subsonic flows. However, starting with the pioneering work of Mack on compressible linear stability theory (cf. [1]), the use of parabolized stability equations [2, 3], direct numerical simulations [4] and experimental work (e.g. [5, 6]) focusing on generic flows over flat plates or cones, considerable progress has been achieved within the past several years (cf. [7]). When additional features, such as shock induced separation by an oblique shock come into play, it can no longer be expected that the parallel-flow assumption typically used in linear stability theory is justified and that investigations other than DNS or experiments yield further insight.

Based on earlier successful investigations by Eißler & Bestek [8] on flat-plate boundary layer transition in zero-pressure gradient boundary layers the present work aims at continuing that work for cases where an impinging shock generates a separation bubble in a laminar boundary layer. As a first step towards DNS of transition in shock-induced separation bubbles, the method developed by Eißler is validated for computations of flow fields including shocks by comparisons with literature and the influence of oblique shocks with different strengths on a small-amplitude Tollmien-Schlichting wave is then investigated. Since it turned out that non-parallel effects are considerably larger than in subsonic flows, the original case of Eißler at M=4.8 had to be reconsidered in order to assess the magnitude of these effects.

New Results in Numerical and Experimental Fluid Mechanics III,
Contributions to the 12th STAB/DGLR Symposium Stuttgart, Germany 2000
S. Wagner, U. Rist, H.-J. Heinemann, R. Hilbig (Eds.)
Notes on Numerical Fluid Mechanics 77, Springer-Verlag 2002
pp. 153-160

2 Numerical method

In order to numerically solve the two-dimensional conservative formulation of the Navier-Stokes equations, spatial streamwise (x) and wall-normal (y) derivatives are approximated by split-type compact finite differences of at least 4th-order accuracy [9]. Dissipative terms in y-direction are discretized by 4th-order-accurate central differences. For the time-evolution, a standard 4-step Runge-Kutta scheme is used (for more details and earlier validations see [10], [11]). Due to the existence of very large gradients caused by the shock, finite difference schemes tend to yield oscillations. To suppress these oscillations, an implicit filter of 4th-order accuracy [12] is implemented in x-direction.

The basic setup of the problem is shown in figure 1 by a visualization of the resulting density gradients (computed Schlieren image) for the case with $Ma = 4.8$ and a shock angle of $\sigma = 13.2^o$. At the inflow boundary, which is indicated in figure 1 as line $A - B$, solutions of the compressible boundary-layer equations are held constant, while the flow variables at the outflow boundary (figure 1, $C - D$) are calculated under neglection of second derivatives in streamwise direction. For the conditions at the wall (figure 1, $A - D$), temperature can be chosen as a constant value or distributed adiabatically. The perturbation of the flowfield origins at the wall. Variations of $(\rho v)'$ (prime denotes disturbance quantities) simulates blowing and suction. The perturbation follows a sine-function multiplied with a Gaussian:

$$f_{\rho v}(\varsigma,t) = \hat{a} * \sin(\omega t) * \sin(n\varsigma) * e^{-b\varsigma^2}, -2\pi \leq \varsigma \leq 2\pi, \tag{1}$$

where n and the length of the disturbance strip is chosen to exactly excite one single wave length, which can be found by linear stability theory. Flow variables at the freestream boundary ($B - C$) are calculated by means of a characteristic condition [10]. The shock is prescribed at the freestream boundary using Rankine-Hugoniot relations to calculate flow variables behind the shock. Hence, flow variables are held constant around the shock along the upper boundary. This explains why a small steady disturbance enters through the upper boundary until it is swept away in downstream direction (cf. figure 1). In the plots within this paper, the local Reynolds number is $R_x = \sqrt{x * \rho_\infty u_\infty / \mu_\infty}$. The perturbed flowfield is excited with the disturbance frequency $F = (2\pi f \mu_\infty)/(u_\infty^2 \rho_\infty)$. The pressure of the flow field p and the disturbance amplitude of the wall pressure $|p'_w|$ is non-dimensionalized by $\rho_\infty u_\infty^2$. For purpose of comparison with validation data, wall pressure p_w in figure 2 is normalized by the wall pressure upstream of the area of influence of the impinging shock. Flow velocities u and v are normalized with free-stream velocity u_∞ and T with the free-stream temperature T_∞. For profiles of flow variables and amplitude distributions a similarity coordinate $\eta = y * 10^5 / R_x$ is used.

3 Results

3.1 Unperturbed laminar boundary layer

Although the focus of our work is on unsteady disturbances at $Ma = 4.8$, comparisons with [13] and [14] for $Ma = 2$ with freestream temperature $T_\infty = 320K$, total pressure in freestream $p_t = 0.1995bar$, shock angle $\sigma = 32.58^o$ and adiabatic wall will be presented here, because suitable steady data for validating the unperturbed flow-field at higher Ma-numbers was not available.

In figure 2, δ_0^* is the displacement thickness at location x_0 where the shock would hit the plate in the inviscid case. The difference to the experimental results regarding the length of the separation bubble which can be identified by its negative skin friction might be caused by the Stanton probe used in the experiments [13] which contacted the wall and thus disturbed the boundary layer. Wall pressure agrees well with both [13] and [14], so do velocity profiles (not presented here).

We now turn to simulations for $Ma = 4.8$ and increasing shock strengths, i.e. $\sigma = 12.5^o$ and $\sigma = 13.2^o$. The other parameters of the flow are $T_\infty = 55.4K$ and $p_t = 4bar$. Wall temperature is held constant at $T_w = 270K$. A typical grid for these simulations consists of 801x151 grid-points. Some interesting details of the flow field can be seen in the computed Schlieren image in Figure 1. The oblique shock, which impinges on the boundary layer turns into a normal shock when approaching the sonic line in the boundary layer. The initial reflection consists of an expansion fan emanating from the impingement location of the shock on the sonic line. It turns into downstream direction as it leaves the boundary layer. Behind the expansion, a recompression is observed which becomes the reflected shock in the far field.

Here, inviscid shock impingement is at $R_{x0} = 1400$. For the case with $\sigma = 13.2^o$ presented in figure 3, the shock angle is strong enough to force separation, which can be identified as an area of negative skin friction while for $\sigma = 12.5^o$, it is not yet sufficient to cause the boundary layer to separate.

For $R_x = 1330$ in figure 4 the different wall-normal profiles for velocity v and pressure p show significant quantitative differences, especially when passing the impinging shock. For the stronger shock these effects are more pronounced, but profiles also differ for u. The same can be seen for $R_x = 1440$ in figure 4. Note the different behaviour of v and p compared to $R_x = 1330$.

Let us now take a closer look into the flow field and what should be expected in terms of stability behaviour. For this, let us draw our attention once again on the computed Schlieren image of the case with $\sigma = 13.2^o$ in figure 1. The pressure gradient which results from the impinging shock causes the boundary layer to thicken. Upstreamward of the shock, the fluid motion is delayed and heated by the compression waves, which result from the deflection of the flow due to this thickening. In the first mode instability region (see [1]), delayed and heated flows are known to cause increasing amplification rates. In contrast, acceleration and cooling yields reduced amplification. This is the case downstream of the shock, where an expansion fan is located. Further downstream a set of compression waves can be identified, which are due to the re-deflection of the flow. This is more pronounced, the more the boundary layer thickens which is directly influenced by the strength of the impinging shock.

3.2 Perturbed laminar boundary layer

For the cases presented in this section we discuss the disturbance waves introduced by activation of the disturbance strip at the wall with $n = 13.5$ (see equation 1). The disturbance strip ranges from $R_x = 477$ to $R_x = 970$. Figure 5 shows fourier transforms of wall pressure disturbances over one perturbation cycle for the different cases. The disturbance frequency was chosen close to the highest amplification upstream of the impinging shock for a two-dimensional first mode instability according to [1].

Up to $R_x = 977$, the disturbance strip can be identified. Compared to [10] our disturbance strip extends over a much larger distance in streamwise direction. This is a possible means to excite a single Tollmien-Schlichting instability mode more precisely than in [10], where two modes were excited with the same disturbance frequency. For $\sigma = 12.5^o$ it can be seen that the influence of the shock causes the Tollmien-Schlichting wave to rise, which results in an increased amplification

rate. After reaching a peak value, the amplitude is decreasing, yielding negative amplification, later increasing again to a positive amplification rate. Figure 6 compares the pressure and the temperature at a location parallel to the wall near the sonic line at the impingement point of the shock, as well as the wall-pressure amplitudes in the same sector. It can be seen that the local amplitude maxima's location corresponds well with the location of the highest temperature peak and a local peak in the pressure distribution which is caused by the impinging shock. This is in accordance with the general behaviour of a heated and delayed flow, which are both known to cause amplification in the region of first mode instability, as stated before.

Linear stability theory did not deliver satisfying results for the amplification curves shown in figure 5. For the case without shock we could show non-parallel effects, which rendered some differences to linear theory (to be explained later in this section). With the shock, there is a deflection of the flow caused by the shock itself. The magnitude of velocity normal to the wall thus reaches larger amounts (see figure 4) which we interpret as a higher degree of non-parallelism. Turning to the stronger shock ($\sigma = 13.2^o$), the area of upstream influence is bigger than before and the wall-pressure disturbances rise to a ten times higher level. Downstream the shock, areas of rise and decrease can be observed. This behaviour is not yet clear and has to be investigated further.

Figure 7 gives normalized amplitude distributions for u, v and p at location $R_x = 1330$. Shapes are almost congruent for tangential velocity u when comparing the case without impinging shock wave and $\sigma = 12.5^o$. But amplitude distributions do differ significantly for the normal velocity v and pressure p. This is the case for $\sigma = 13.2^o$, as well. However, differences for u can be observed here, too. It is especially interesting to note here that the secondary amplitude maxima which are further away from the wall than the primary ones are decreasing with increasing shock strength. This lies in accordance with the observations of non-parallel effects and a stronger amplification at closer distance to the wall.

Figure 8 shows amplification rates of second wall-normal maxima of the disturbance amplitudes for a boundary-layer flow at $Ma = 4.8$ without impinging shock, which are located in a farther position normal to the wall than first maxima. For comparison, results of linear theory and simulations of an idealized, parallel boundary layer profile at discrete locations R_x are shown. Amplification rate is $\alpha_i = -(\partial ln(A(x)/A_0))/(\partial x)$, where $A(x)/A_0$ is the amplitude ratio of the concerning flow variable, respectively, and $x = R_x^2 * 10^{-5}$. For the given frequency, our integration domain covers both the first and second mode instability domains [1]. The second instability mode starts to grow at $R_x \approx 1500$. In linear theory both instability regions are separated by a shallow region with $\alpha_i > 0$. However, in DNS this is not the case, due to large non-parallel effects, which were not documented before.

Linear theory (see [1]) gives one single amplification rate for each flow variable everywhere in the boundary layer. To prove that the differences in our simulations are really caused by non-parallelism (linear stability theory assumes parallel flow), simulations were carried out using an idealized, parallel boundary layer at discrete locations R_x. These results agree well with linear theory.

Conclusions and future research

Shock/boundary layer interaction imposes adverse and favourable local pressure and temperature gradients on the boundary layer apparently leading to considerable amplification of small-amplitude Tollmien-Schlichting waves. Non-parallel effects become increasingly large with growing shock strength. Future research aims at explaining the influence of three-dimensional and

large-amplitude disturbances on the transition process as well as other unsteady phenomena in the flow-field.

Acknowledgement

The authors would like to thank the DFG for supporting this research within SFB259.

References

[1] Mack, L., Boundary layer stability theory. *Jet Propulsion Laboratory, Pasadena, Tech. Rep.*, 900-277 (1969).

[2] Hein, S., Bertolotti, F., Simen, M., Hanifi, A. and Henningson, D., Linear nonlocal instability analysis – the linear NOLOT code –. *DLR-IB*, 223-94 A56 (1994).

[3] Pruett, C., A comparison of PSE and DNS for high-speed boundary-layer flows. *Transitional and Turbulent Compressible Flows, L.D. Kral and T.A. Zang (eds.)*, FED Vol. 151, ASME, New York, 57–67 (1993).

[4] Eißler, W. and Bestek, H., Direct numerical simulation of transition in Mach 4.8 boundary layers at flight conditions. *Engineering Turbulence Modelling and Experiments*, 3, 611–620 (1996).

[5] Kosinov, A., Maslov, A. and Shevelkov, S., Experiments on the stability of supersonic boundary layers. *J. Fluid Mech.*, 219, 621–633 (1990).

[6] Stetson, K. and Kimmel, R., On hypersonic boundary-layer stability. *AIAA Paper*, No. 92-073 (1992).

[7] Saric, W., Reshotko, E. and Arnal, D., Hypersonic Laminar-Turbulent Transition. *AGARD*, AR-319 (1998).

[8] Eißler, W. and Bestek, H., Spatial numerical simulations of linear and weakly nonlinear wave instabilities in supersonic boundary layers. *Theoret. Comput. Fluid Dynamics*, 8, 219–235 (1996).

[9] Kloker, M., A Robust High-Resolution Split-Type Compact FD Scheme for Spatial Direct Numerical Simulation of Boundary-Layer Transition. *Applied Scientific Research*, 59, 353–377 (1998).

[10] Eißler, W., *Numerische Untersuchungen zum laminar-turbulenten Strömungsumschlag in Überschallgrenzschichten*. Dissertation, Universität Stuttgart (1995).

[11] Fezer, A. and Kloker, M., Transition Process in Mach 6.8 Boundary Layers at Varying Temperature Conditions Investigated by Spatial Direct Numerical Simulation. *Notes on Numerical Fluid Mechanics, Vieweg*, 72, 138–145 (1999).

[12] Lele, S., Compact Finite Difference Schemes with Spectral-like Resolution. *J. Comp. Phys.*, 103, 16–42 (1992).

[13] Hakkinen, R., Greber, J., Trilling, L. and Abarbanel, S., The interaction of an oblique shock wave with a laminar boundary layer. *NASA MEMO*, 2-18-59W (1959).

[14] Katzer, E., On the lengthscales of laminar shock/boundary-layer interaction. *J. Fluid Mech.*, 206, 477–496 (1989).

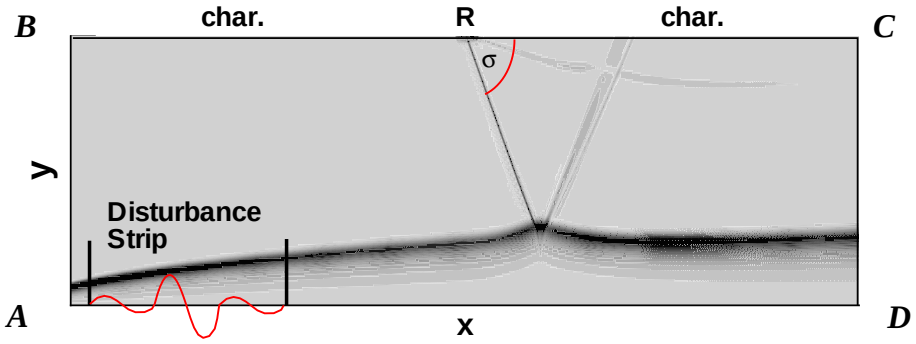

Figure 1 Integration domain (square $A-B-C-D$), disturbance strip and computed Schlieren image ($\mid \partial\rho/\partial y \mid$) for $Ma = 4.8$, $\sigma = 13.2^o$, $R_{x0} = 1397$.

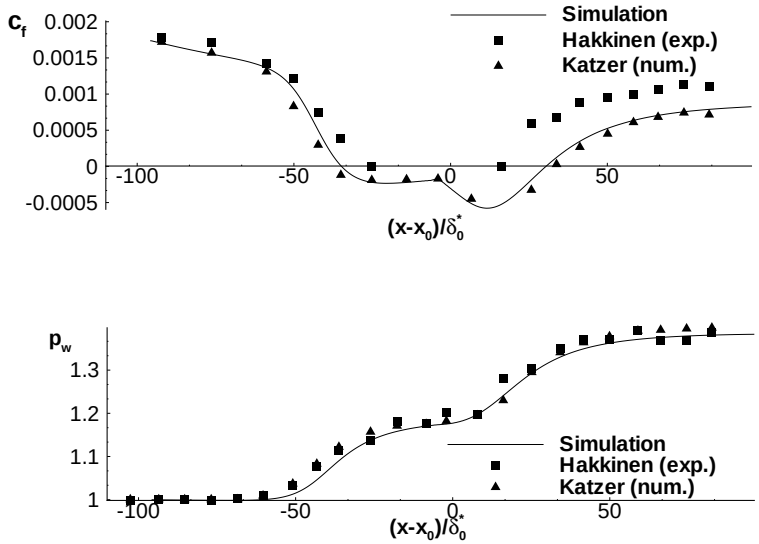

Figure 2 Comparison of skin friction (upper image) and wall pressure (lower image) at $Ma = 2$. $R_{x_0} = 548$.

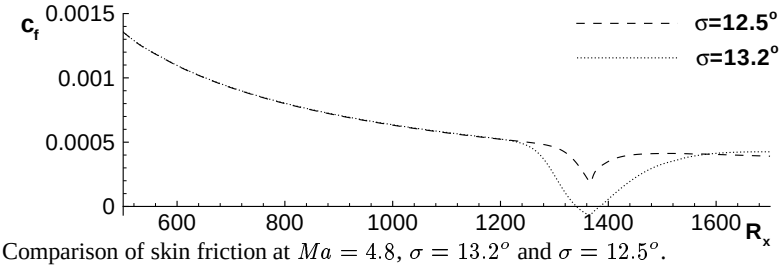

Figure 3 Comparison of skin friction at $Ma = 4.8$, $\sigma = 13.2^o$ and $\sigma = 12.5^o$.

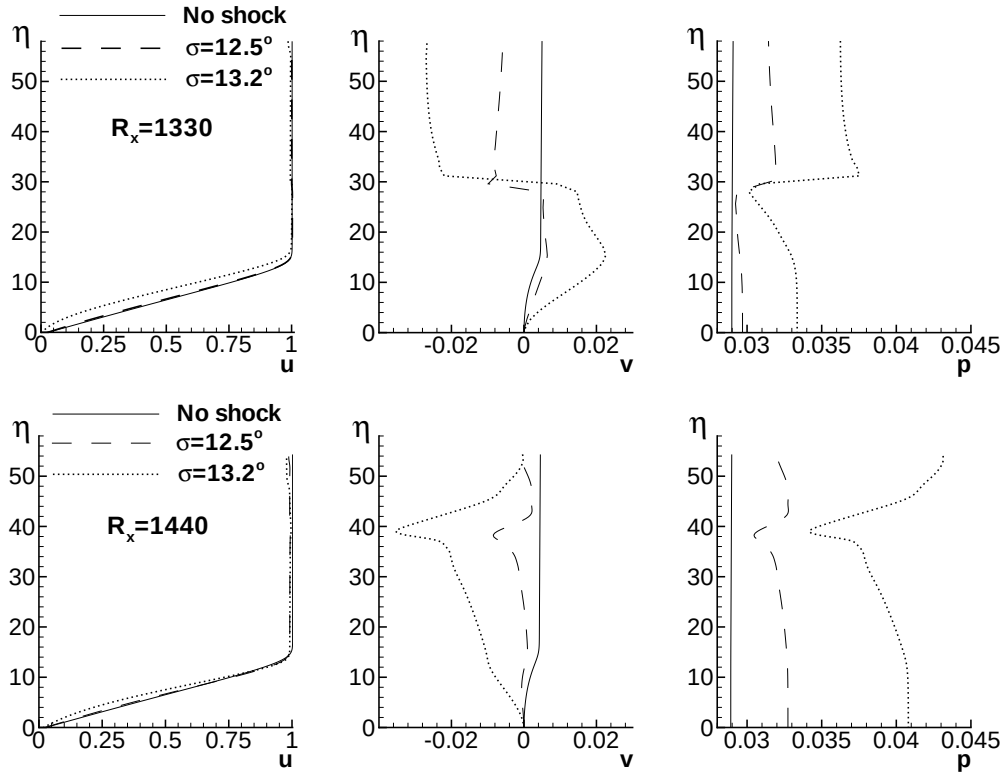

Figure 4 Profiles of flow variables at locations $R_x = 1330$ and $R_x = 1440$.

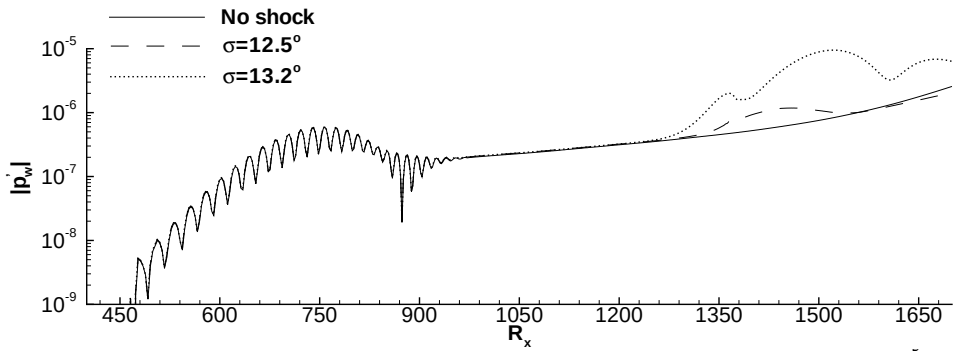

Figure 5 Comparison of pressure disturbance amplitudes, disturbance frequency $F = 10 * 10^{-5}$.

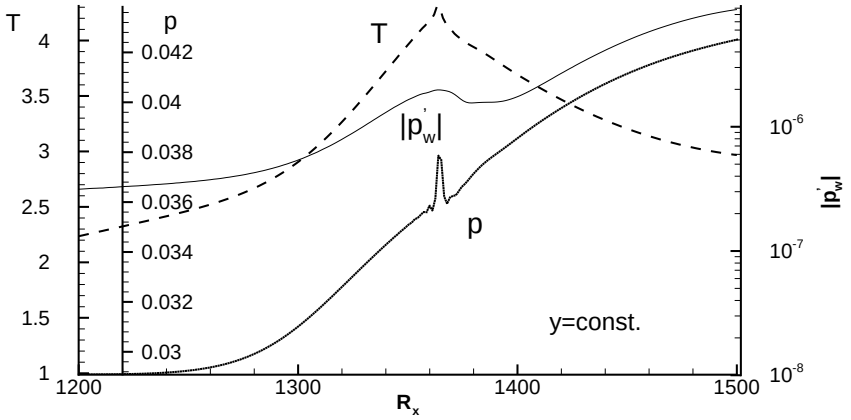

Figure 6 Temperature T, pressure p parallel to the wall near sonic-line at impinging shock as well as wall-pressure amplitudes in a sector of the flow-field for $\sigma = 13.2^o$.

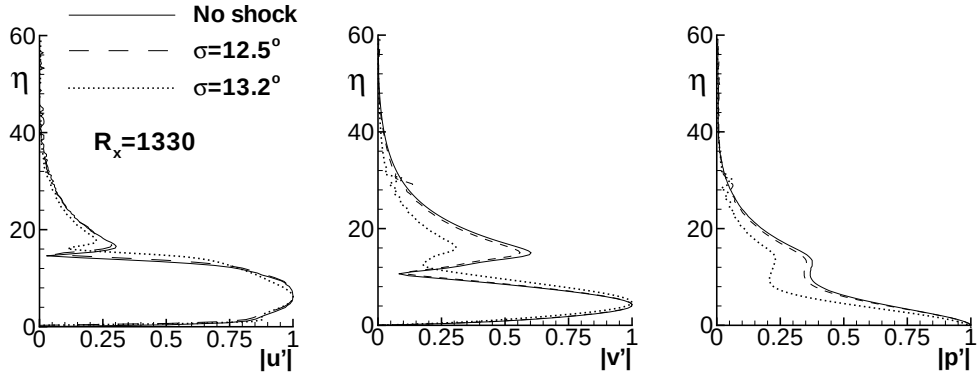

Figure 7 Profiles of amplitude distributions of flow variables at $Ma = 4.8$. Disturbance Frequency $F = 10 * 10^{-5}$. Amplitude distributions are normalized with absolute maxima of each flow variable.

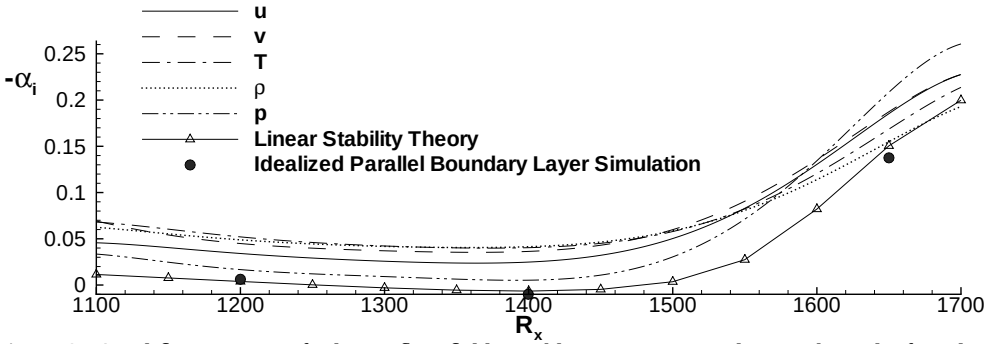

Figure 8 Amplification rates of relevant flow-field variables at $Ma = 4.8$ along with results from linear stability theory and simulation of idealized boundary layer. No impinging shock.